JOURNAL OF SOLID STATE CHEMISTRY 88, 45–52 (1990)

Electronic Structure of Transition Metal Compounds: Photoemission Experiments and Model Hamiltonian Calculations

D. D. SARMA

Solid State and Structural Chemistry Unit, Indian Institute of Science, Bangalore-560 012, India

Received May 2, 1990

DEDICATED TO J. M. HONIG ON THE OCCASION OF HIS 65TH BIRTHDAY

We discuss the case of NiO in detail to exemplify the use of photoemission experiments and model Hamiltonian calculations in order to unravel the electronic structure of transition metal compounds. Then we discuss the transition metal compounds and their metallic/nonmetallic properties in terms of a generalized phase diagram as a function of the Coulomb interaction strength and charge transfer energy. Finally, we discuss the electronic structure of the high-T_c cuprate superconductors as deduced from photoemission experiments and model calculations in relation to the above-mentioned phase diagram.

Introduction

The transition metal compounds manifest a very spectacular range of electronic and magnetic properties, encompassing such diverse aspects as superconductivity, magnetism (ferro- as well as antiferromagnetism), spin-state transition, and metal–nonmetal transition. Even in the very limited class of the transition metal monoxides in the rock-salt structure (TiO–NiO), very different behaviors are found. For example, the monoxides of the lighter transition metals (Ti and V) are metallic, whereas the MnO, CoO, and NiO are antiferromagnetic insulators. The insulating properties of NiO, in fact, have been discussed over the last four decades and have been a consistent source of animated controversy. This compound was considered (*1*) to be the original Mott insulator; a large intra-3*d* Coulomb interaction strength (U_{dd}) of 6 eV (or larger) (*2–5*) is suggested to separate the occupied part of Ni 3*d* levels (the lower Hubbard band) from the unoccupied part (the upper Hubbard band). However, later band structure calculations (*6*) suggested that the insulating nature of this compound is derived not from U_{dd} but from exchange and crystal field splittings. While a considerable effort (*7–20*) has been devoted in understanding the electronic structure of NiO employing various photoemission techniques, the interpretations of the various features observed were not unambiguous for quite some time. We shall discuss in detail here the present understanding of the electronic structure of NiO.

The various discussions to understand the electronic structure of NiO have naturally contributed to the understanding of the properties of the other transition metal com-

0022-4596/90 $3.00

pounds, in general. In fact, a phase diagram has been suggested (*21*) where the various kinds of insulating as well as metallic transition metal compounds are properly classified in terms of the strength of U_{dd} and the charge transfer energy between the transition metal d and the oxygen p ($\Delta = \varepsilon_d - \varepsilon_p$). We shall discuss this diagram, including some important changes to it that have been suggested (*22*) recently. In relation to this phase diagram, we shall discuss the electronic structure of the high-T_c cuprate superconductors as obtained from the photoemission experiments.

Results and Discussion

Some of the most significant contributions to the understanding of the electronic structure of NiO have come from the proper assignments and interpretation of the photoemission (and other related techniques) spectra of this compound (*14–16, 19, 20*). We show the X-ray photoelectron spectrum of NiO in Fig. 1. The first important realization (*14, 15*) was the fact that the ligand field theory cannot explain the features over the entire spectral range. It was necessary (*14, 15*) to take explicity into account the ligand (i.e., O 2*p*)–metal (Ni 3*d*) hybridization and the intraatomic Coulomb interaction, U_{dd}, in order to satisfactorily explain the spectral features. This was done approximating the bulk NiO by a cluster $(NiO_6)^{10-}$. The ground state wave function ψ_g of this cluster is given by

$$\psi_g = a|d^2L^0> + b|d^1L^1> + c|d^0L^2>,$$

where $|d^2L^0>$ (in the hole configuration) denotes the ionic $Ni^{2+}O^{2-}$ (or the $3d^8 2p^6$) state, $|d^1L^1>$ represents the $Ni^{1+}O^{1-}$ (or the $3d^9 2p^5$) state, and $|d^0L^2>$ is the $3d^{10}2p^4$ state. The hybridization between the Ni 3*d* and O 2*p* states mixes the $|d^2L^0>$, $|d^1L^1>$, and $|d^0L^2>$ states in order to substantially lower the energy of the ground state compared to the ionic state $|d^2L^0>$ or the $Ni^{2+}O^{2-}$ state.

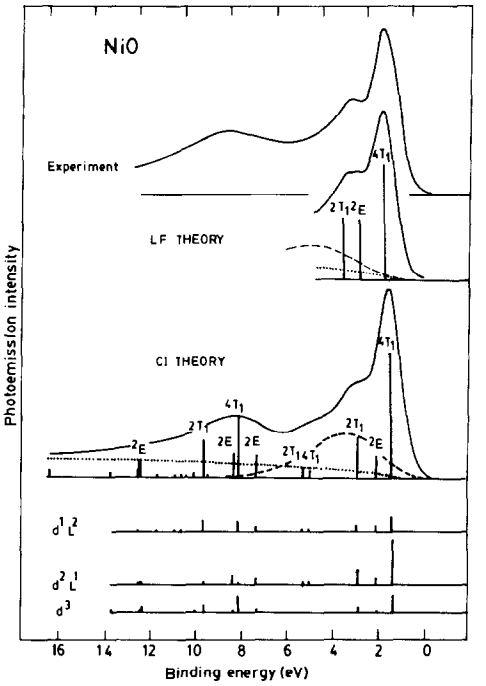

FIG. 1. The comparison of the experimental photoemission spectrum of NiO in the valence band region with the spectra calculated within the ligand field (LF) and configuration interaction (CI) theories (adopted from Ref. (*14*)). The experimental spectrum is from S. P. Kowalczyk, L. Ley, R. A. Pollack, and D. A. Shirley, cited in B. H. Brandow, *Adv. Phys.* **26,** 651, 1977.

This covalency effect plays an important role in determining the electronic structure of NiO. Assuming the contribution of $|d^0L^2>$ in ψ_g to be small due to energetic reasons and neglecting its effects, it was found (*14*) that the ground state has the total symmetry $^3A_{2g}$. This implies that the $3d^8$ configuration ($|d^2L^0>$) with $|t_{2g\uparrow}^3 t_{2g\downarrow}^3 e_{g\uparrow}^2, {}^3A_{2g}>$ hybridizes with various $|d^1L^1>$ configurations with the same symmetry to form the ground state wave function. The final state following the photoemission has one less electron (or one extra hole) and consequently, the final state wave function is given as

$$\psi_f = d|d^3L^0> + e|d^2L^1> + f|d^1L^2>.$$

Since the initial state has the $^3A_{2g}$ symmetry, the final states can have ^2E_g, $^2T_{1g}$, and $^4T_{1g}$ symmetries due to the selection rules. The corresponding $3d^7$ (or $|d^3L^0>$) configurations are given by $|t_{2g}^6 e_g^1, {}^2E_g>$, $|t_{2g}^5 e_g^2, {}^2T_{1g}>$, and $|t_{2g}^5 e_g^2, {}^4T_{1g}>$; the $|d^2L^1>$ and $|d^1L^2>$ states also are chosen with the proper symmetries. Estimating the transfer integrals from band structure calculations (*23*) and using the various energies (e.g., U_{dd} and Δ) as fitting parameters, the photoemission spectrum for this $(NiO_6)^{10-}$ cluster was calculated (*14*). The result is shown in Fig. 1. From the comparison between the experimental and the calculated spectra, it is obvious that the fit is very good. From the best fit, the charge transfer energy, Δ, was estimated to be -3.5 eV and U_{dd} was estimated to be 8–10 eV. It is worthwhile to notice that the estimate of Δ is in agreement with the value estimated earlier from an analysis of the core level spectra (*24*).

The most interesting conclusion arrived at in Ref. *14* and *15* is that the most prominent, lowest binding energy peak in the NiO photoemission spectra is primarily due to final states with a d-hole from $3d^8$ configuration (i.e., $|d^3L^0>$) screened by a $L \rightarrow d$ electron transfer (i.e., $|d^2L^1>$ state). This is in contrast to the previously held belief that the leading sharp peak is due to the photoemission from the $3d^8$ state leading to a final $3d^7$ state. The unexpected result that the most prominent leading peak is primarily due to the photo-hole in the ligand levels arising out of screening can be clearly seen in the lower part of Fig. 1 where the relative contributions of each of the three basis configurations ($|d^3L^0>$, $|d^2L^1>$, and $|d^1L^2>$) are given. It is also seen that the $3d^7$ configuration ($|d^3L^0>$) contributes considerable intensity in the satellite region of the spectrum around 6–12 eV binding energy.

With this changed interpretation of the photoemission spectrum of NiO, several studies (*16–20*) immediately followed reporting the occupied as well as the unoccupied part of the valence band region in NiO, as obtained from photoemission and inverse-photoemission (or bremsstrahlung isochromat) techniques. In Fig. 2 we show some of the representative spectra of NiO both in the occupied and the unoccupied regions. The leading peak in the occupied part of the valence band region (obtained with photoemission), as discussed previously, is attributed to the primarily $|d^2L^1>$ state with a hole in the ligand levels. The unoccupied part of the valence band region obtained by the inverse photoemission techniques will have $|d^1L^0>$ and $|d^0L^1>$ states admixed, since it corresponds to an electron addition final state from the initial state ($a|d^2L^0> + b|d^1L^1>$). The leading peak in the inverse photoemission spectra of NiO near-

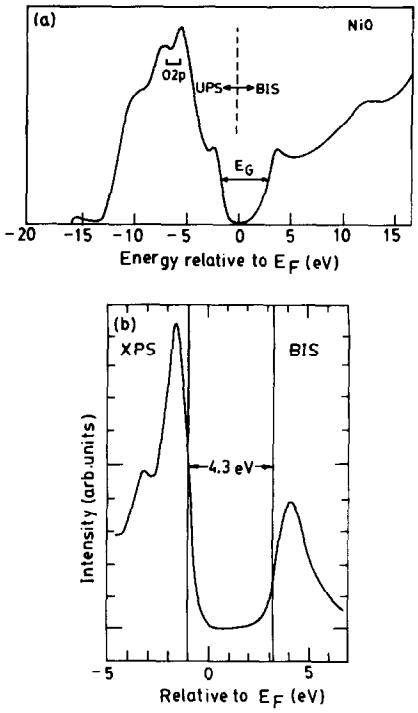

FIG. 2. (a) UV photoemission spectrum (UPS) and the bremsstrahlung isochromat spectrum (BIS) of NiO showing the band gap (from Ref. (*16*)). (b) X-ray photoemission spectrum (XPS) and BIS of NiO (from Ref. (*20*)).

est to the Fermi energy has been attributed (*16, 20*) to a primarily $|d^1L^0>$ state. Thus the energy difference between the $|d^2L^1>$ state below E_F and the $|d^1L^0>$ state above E_F is about 4.3 eV. Then this is the minimum energy required to cause a charge fluctuation in the NiO lattice, if interatomic Coulomb interaction effects can be neglected. The success of these spectroscopic techniques in elucidating the electronic structure of NiO is in providing the microscopic origin of the bandgap which is also measured (*25, 26*) to be at least 3 eV from resistivity data. Moreover, the optical absorption spectrum of NiO also indicates (*2*) an optical bandgap of about 4 eV. From the above discussion of the characters of the features closest to E_F in photoemission and the inverse photoemission spectra in NiO (Figs. 1 and 2), it is evident that the 4-eV bandgap has a substantial O $2p$–Ni $3d$ charge transfer nature. This is evident since the lowest energy final state after the removal of an electron is essentially a $|d^2L^1>$ state and after the addition of an electron it is a $|d^1L^0>$ state. However, there are important admixtures of the other states (e.g., $|d^1L^2>$ and $|d^3L^0>$ configurations) into the leading peak of the photoemission spectrum (Fig. 1). This ensures a somewhat mixed character of the bandgap in NiO.

The spectra shown in Figs. 1 and 2 also provide a measure for the U_{dd} in NiO. It is to be noted that the satellite feature in the photoemission (about 8 eV below E_F) has substantial $3d^7$ character (i.e., $|d^3L^0>$ final state in photoemission). Then the energy difference between this peak and the lowest energy peak in the inverse photoemission spectra (at about 4 eV above E_F) arising from the $3d^9$ configuration is related to U_{dd}. However, it must be realized that this energy difference is not equal to U_{dd}, since there is substantial contribution to energy shifts due to extensive hybridization. When corrected for this hybridization shift employing detailed model calculations, a U_{dd} value between 7 and 9 eV has been deduced

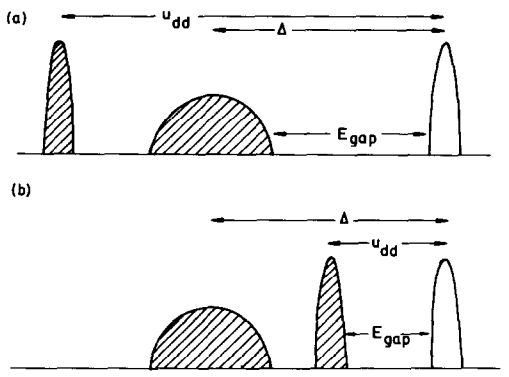

FIG. 3. (a) The schematic representation of the electronic structure of the late transition metal oxides (e.g., NiO), illustrating a charge-transfer insulator. (b) The schematic representation of the electronic structure of the early transition metal insulating oxides (e.g., VO_2), illustrating a Mott–Hubbard insulator.

(*20*). This is in good agreement with estimate of U_{dd} obtained (*14*) only from the photoemission data. Using the various energetics, e.g., the charge transfer energy, Δ, of −3.5 eV and the U_{dd} of about 9 eV, we show schematically the electronic structure of NiO in Fig. 3. In Fig. 3a we show it in the absence of any hybridization interaction between Ni $3d$ and O $2p$. In this case, the $3d$ band from the Ni sublattice splits into the upper and the lower Hubbard bands separated by U_{dd}. Since the total degeneracy of the e_g level is four, each of the Hubbard bands can accommodate two electrons for every Ni (beyond the six electrons in the filled t_{2g} band). Thus, in the ionic limit of $Ni^{2+}O^{2-}$ with $3d^8$ configuration, the lower Hubbard band is fully filled and the upper Hubbard band is entirely empty. The oxygen $2p$-derived broad band is within the gap between the two Hubbard bands and is filled. The energy difference between the filled oxygen p band and the empty upper Hubbard band is the charge transfer energy. Turning on the interaction between Ni $3d$ and O $2p$, while causing very important shifts to the various energy differences,

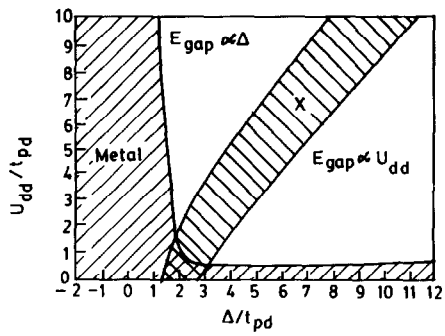

FIG. 4. The schematic phase diagram for the transition metal compounds in the U_{dd}–Δ plane (adopted from Ref. (*21*)). The Mott–Hubbard insulator regime has E_{gap} approximately proportional to U_{dd}, while the charge-transfer insulator shows an E_{gap} proportional to Δ. In the region X, the gap has a mixed character.

does not change the overall picture shown in Fig. 3a. From this figure, it is clear that for small hybridization interactions, the bandgap in NiO would be of a charge-transfer nature; however, strong hybridization leads to extensive mixing of different states giving rise to a bandgap of mixed nature in NiO. This is in contrast to the classical Mott-insulator interpretation of NiO, where the bandgap is dictated by the U_{dd} alone. It is also obvious from the schematics in Fig. 3, that the bandgap will have a charge-transfer nature whenever $U_{dd} \gg \Delta$. However, if $\Delta \gg U_{dd}$ (shown in Fig. 3b), the bandgap is between the lower and the upper Hubbard bands and the system behaves like the classical Mott–Hubbard insulator. Using these concepts, a phase diagram has been proposed (*21*) for the electronic structure of the transition metal compounds in general. This phase diagram is shown in Fig. 4. From this diagram it is seen that the compound is metallic, whenever either U_{dd} or Δ is very small. With small U_{dd}, the lower and the upper Hubbard bands overlap (Fig. 3b with $E_{gap} = 0$), and one obtains a d-band metallic behavior. However, for a large U_{dd} and a small Δ (Fig. 3a with a vanishing gap), one obtains a p-band metalic behavior. Within the insulating regime, a diagonal boundary (region X in Fig. 4) in the U_{dd}–Δ plane approximately divides the charge transfer insulators from the Mott–Hubbard insulators. It should however be realized that the boundary region X is merely notional and the changeover from the Mott–Hubbard regime to the charge transfer regime takes place continuously, with mixed character bandgap around the boundary, for any finite value of the hybridization interaction.

With the help of the phase diagram in Fig. 4 and the above discussion, one can now classify the transition metal compounds. For example, the late transition elements in the 3d series are characterized by considerably larger U_{dd} compared to the early transition elements (*28*). Moreover the charge transfer energies in the late transition metal oxides tend to be small compared to U_{dd}. Thus, these insulating compounds (e.g., NiO, CuO, etc.) are primarily charge transfer insulators. With the lighter transition metal monoxides, e.g., TiO and VO, one has the situation of a small U_{dd} and a large Δ, leading to a d-band metallic behavior. The transition metal oxides in the middle of the period (i.e., Mn and Fe oxides) already have a substantial U_{dd} (partly enhanced by the half-filled or nearly half-filled 3d-shell configurations) and a smaller Δ. This makes these oxides closer to charge transfer insulator regime; however, these are closer to the boundary region X in Fig. 4 and are expected to show somewhat mixed behavior. The insulating phases of V_2O_3 and VO_2 are expected to be Mott–Hubbard insulator, close to the dividing line between the metal and the insulating regime. On the other hand, NiS_xSe_{2-x} which exhibits metal–insulator transition is expected to be close to the metal–nonmetal boundary within the charge transfer regime.

Recently it has been shown (*22*) that there are a few important modifications required to the above-mentioned phase diagram for the case of transition metal compounds,

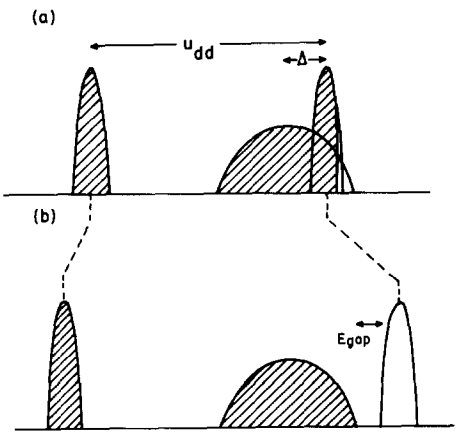

FIG. 5. The schematic representation of a covalent insulator. (a) In the absence of hybridization, a small Δ compared to the ligand bandwidth will give rise to a metallic state. (b) A sizable hybridization can open up a gap for the situation in (a), leading to the formation of a covalent insulator.

which often have strong covalent bonds (i.e., a large hybridization interaction and a small Δ). In the presence of a sizable hybridization strength between the 3*d* and the oxygen 2*p*, it was shown that the metal–nonmetal boundary that is nearly parallel (*21*) to the U_{dd} axis shifts significantly closer to the U_{dd} axis. This opens up a further insulating phase at smaller Δ-values, as compared to the phase diagram proposed earlier (*21*). Moreover it has been shown that the properties in this highly covalent region cannot be described merely in terms of U_{dd}/t_{pd} and Δ/t_{pd} (as stipulated for the phase diagram in Fig. 4), but the explicit value of the t_{pd} plays the crucial role in determining the metallic or the insulating property. This situation is schematically shown in Fig. 5. In the presence of small Δ, such that the oxygen *p*-band overlaps the upper Hubbard band, the system will show metallic behavior, when t_{pd} is small (Fig. 5a). However, as t_{pd} increases, the two overlapping bands will separate out due to covalency effects at the same Δ-value leading to an insulating behavior (Fig. 5b). This insulating regime has been termed (*22*) the covalent insulator to distinguish it from the change transfer insulator which occurs at a larger Δ-value. The main distinguishing feature between these two insulating phases is that while the insulating behavior of the charge transfer regime is retained in the limit of vanishing t_{pd}, the covalent insulator can exist only at finite t_{pd} and will be metallic in the absence of t_{pd}. It has also been pointed out (*22*) that the compounds like NiS, etc., are better described as a covalent insulator than a charge transfer insulator as was previously thought. In fact it has also been suggested (*22*), that the insulating parent compounds (e.g., La_2CuO_4, Nd_2CuO_4) of the high-T_c cuprate superconductors are in (or close to) the covalent insulating regime, with a very small Δ and a large t_{pd}. This is borne out by most of the band structure calculations (*30*). It should be noticed that the covalent insulating regime necessarily leads to a strong admixture of metal 3*d* and O 2*p* states, giving rise to strongly mixed valent compounds. A large number of core level photoemission spectra from a large variety of cuprate superconductors have recently been analyzed (*31*) within a single simple model; it turns out that the strongly mixed-valent nature of these cuprate superconductors is an inescapable conclusion arising from the core level photoemission data. Thus, the core level photoemission spectra support the notion that the insulating analogues of these high-T_c materials are close to being covalent insulators. In the following we discuss the detailed analysis of the core level photoemission spectrum of La_2CuO_4 as an example.

The undoped stoichiometric insulating La_2CuO_4 has Cu in the formal divalent state. In the model of Ref. (*29*), the Cu is thus considered to be a formal Cu^{2+} impurity in the oxygen sublattice. Since the oxygen–oxygen interaction is substantial in these oxide materials, the consideration of the oxygen sublattice takes into account the

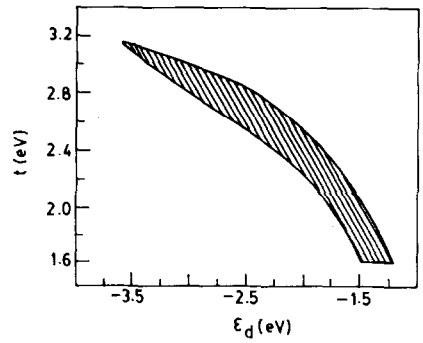

FIG. 6. The range of ε_d and t that can explain the observed core level photoemission spectrum of La_2CuO_4 (from Ref. (29)).

important band structure effects. However, this model does not take into account the Cu sublattice and only considers one Cu impurity. Since the band structure of the two-dimensional lattice of the oxygen atoms with p_x and p_y can be easily solved, the k-dependent hybridization matrix elements $t^i_{d\vec{k}}$ is calculated to be

$$\mathrm{Re}[t^1_{d\vec{k}}] = \frac{1}{2\sqrt{2}} t[-1 - \cos k_a + \cos k_b + \cos(k_a + k_b)]$$

$$\mathrm{Re}[t^2_{d\vec{k}}] = \frac{1}{2\sqrt{2}} t[-1 + \cos k_a - \cos k_b + \cos(k_a + k_b)]$$

It was further found that the core-level photoemission spectrum in the Cu $2p$ region in La_2CuO_4 does not uniquely determine the hybridization strength, t, and the charge transfer energy, Δ. This is more so, when one takes into account the intrinsic experimental uncertainties in estimating the intensities and energy positions of various spectral features. Thus, a range of t and Δ were found to provide satisfactory fit to the experimental data. This range of t and Δ is shown as a shaded region in Fig. 6. From this figure we find that a t-value of 2.5 eV or lower will require the Δ to be larger than -2.4 eV in order to explain the core level photoemission spectra. It should be noted that the values of t_{pp} used in these calculations determine the bottom of the oxygen p band at -2.4 eV. Thus, for reasonable values of t, the d-level position will have to be within the oxygen-derived p band. This indicates that the insulating nature of La_2CuO_4 is due to covalency effects and not due to Δ. Thus, this compound is (or close to being) a covalent insulator.

In the above discussions, we have briefly discussed the electronic structure of NiO as has been established by employing photoemission and other related techniques. The phase diagram in the U_{dd}–Δ plane to characterize the different metallic and insulating phases that are possible for transition metal compounds has been discussed, including some recent modifications in the phase diagram. In light of the new understandings, we have discussed the possibility of the insulating analogues of the high-T_c cuprates (in particular La_2CuO_4) being covalent insulators as distinct from the charge transfer or the Mott–Hubbard insulator.

References

1. N. F. MOTT, *Proc. Phys. Soc. London, Sec. A* **62,** 416 (1949).
2. N. F. MOTT AND Z. ZINAMON, *Rep. Prog. Phys.* **33,** 881 (1970).
3. D. ADLER AND J. FEINLEIB, *Phys. Rev. B* **2,** 3112 (1970).
4. L. F. MATTHEISS, *Phys. Rev. B* **5,** 290 (1972).
5. B. KOILLER AND L. M. FALICOV, *J. Phys. C* **7,** 299 (1974).
6. K. TERAKURA, A. R. WILLIAMS, T. OGUCHI, AND J. KUBLER, *Phys. Rev. Lett.* **52,** 1830 (1984).
7. D. E. EASTMAN AND J. L. FREEOUF, *Phys. Rev. Lett.* **34,** 395 (1975).
8. K. S. KIM AND N. WINOGRAD, *Surf. Sci.* **43,** 625 (1974).
9. G. K. WERTHEIM AND S. HUFNER, *Phys. Rev. Lett.* **28,** 1028 (1972).
10. S. HUFNER AND G. K. WERTHEIM, *Phys. Rev. B* **8,** 4857 (1983).
11. G. K. WERTHEIM, H. J. GUGGENHEIM, AND S. HUFNER, *Phys. Rev. Lett.* **30,** 1050 (1973).

12. M. R. THULER, R. L. BENBOW, AND Z. HURYCH, *Phys. Rev. B* **27,** 2082 (1983).
13. S. J. OH, J. W. ALLEN, I. LINDAU, AND J. C. MIKKELSEN, *Phys. Rev. B* **26,** 4845 (1982).
14. A FUJIMORI, F. MINAMI, AND S. SUGANO, *Phys. Rev. B* **29,** 5225 (1984).
15. A. FUJIMORI AND F. MINAMI, *Phys. Rev. B* **30,** 957 (1984).
16. S. HUFNER, F. HULLIGER, J. OSTERWALDER, AND T. RIESTERER, *Solid State Commun.* **50,** 83 (1984); S. HUFNER, J. OSTERWALDER, T. RIESTERER, AND F. HULLIGER, *Solid State Commun.* **52,** 793 (1984).
17. M. SCHEIDT, M. GLOBL, AND V. DOSE, *Surf. Sci.* **112,** 97 (1981).
18. F. J. HIMPSEL AND TH. FAUSTER, *Phys. Rev. Lett.* **49,** 1583 (1982).
19. J. M. MCKAY AND V. E. HENRICH, *Phys. Rev. Lett.* **53,** 2343 (1984).
20. G. A. SAWATZKY AND J. W. ALLEN, *Phys. Rev. Lett.* **53,** 2339 (1984).
21. J. ZAANEN, G. A. SAWATZKY, AND J. W. ALLEN, *Phys. Rev. Lett.* **55,** 418 (1985).
22. D. D. SARMA, S. NIMKAR, P. P. MITRA, H. R. KRISHNAMURTHY *et al.*, to be published.
23. L. F. MATTHEISS, *Phys. Rev. B* **5,** 290 (1972).
24. G. VAN DER LAAN, C. WESTRA, C. HAAS, AND G. A. SAWATZKY, *Phys. Rev. B.* **23,** 4369 (1981).
25. R. NEWMAN AND R. M. CHRENKO, *Phys. Rev.* **114,** 1507 (1959).
26. M. A. WITTENAUER AND L. L. VAN ZANDT, *Philos. Mag. B* **46,** 659 (1982).
27. R. J. POWELL AND W. E. SPICER, *Phys. Rev. B* **2,** 2182 (1970).
28. T. BANDYOPADHYAY AND D. D. SARMA, *Phys. Rev. B* **39,** 3517 (1989).
29. D. D. SARMA AND A. TARAPHDER, *Phys. Rev. B* **39,** 11,570 (1989).
30. W. E. PICKETT, *Rev. Mod. Phys.* **61,** 433 (1989).
31. D. D. SARMA AND S. G. OVCHINNIKOV, to be published.